APPLIED GEOPHYSICS, Vol.13, No.1 (March 2016), P. 194-202, 8 Figures.
DOI:10.1007/s11770-016-0537-1

Azimuthal cement evaluation with an acoustic phased-arc array transmitter: numerical simulations and field tests*

Che Xiao-Hua[1,2], Qiao Wen-Xiao[1,2], Ju Xiao-Dong[1,2], and Wang Rui-Jia[1,2]

Abstract: We developed a novel cement evaluation logging tool, named the azimuthally acoustic bond tool (AABT), which uses a phased-arc array transmitter with azimuthal detection capability. We combined numerical simulations and field tests to verify the AABT tool. The numerical simulation results showed that the radiation direction of the subarray corresponding to the maximum amplitude of the first arrival matches the azimuth of the channeling when it is behind the casing. With larger channeling size in the circumferential direction, the amplitude difference of the casing wave at different azimuths becomes more evident. The test results showed that the AABT can accurately locate the casing collars and evaluate the cement bond quality with azimuthal resolution at the casing–cement interface, and can visualize the size, depth, and azimuth of channeling. In the case of good casing–cement bonding, the AABT can further evaluate the cement bond quality at the cement–formation interface with azimuthal resolution by using the amplitude map and the velocity of the formation wave.
Keywords: Cement bond quality, phased-arc array transmitter, azimuthal resolution, amplitude, arrival time

Introduction

Evaluations of the cement bond quality are very important to oil production. The cement bond quality can be evaluated by analyzing the acoustic response from the casing–cement interface and the cement–formation interface. Nevertheless, it is difficult to detect the azimuth of cement channeling.

The conventional cement bond log (CBL) and the variable density log (VDL) are well-known conventional acoustic logging tools that are used to evaluate the cement bond quality. The CBL and VDL, because of the omnidirectional radiation characteristics of monopole sources, have no azimuthal detection capability of the cement channeling (Pardue et al., 1963; Bolshakov et al., 2010; Qiao et al., 2011). The segmented bond tool (SBT) uses six pads and twelve transducers to evaluate

Manuscript received by the Editor June 20, 2015; revised manuscript received January 2, 2016.
*This study was supported by the National Natural Science Foundation of China (Nos. 11204380, 11374371, 61102102, and 11134011), National Science and Technology Major Project (No. 2011ZX05020-009), China National Petroleum Corporation (Nos. 2014B-4011, 2014D-4105, and 2014A-3912) and PetroChina Innovation Foundation (No. 2014D-5006-0307).
1. State Key Laboratory of Petroleum Resources and Prospecting, China University of Petroleum, Beijing 102249, China.
2. Key Laboratory of Earth Prospecting and Information Technology, Beijing 102249, China.

the cement integrity (Bigelow et al., 1990). The SBT can only evaluate the cement bond quality at the casing–cement interface with azimuthal resolution of approximately 60° and VDL is used to determine the cement bonding at the cement–formation interface. The isolation scanner (Schlumberger) is a new-generation cementing evaluation tool that combines ultrasonic reflection and refraction with significant improvements for lightweight cementing (van Kuijk et al., 2005; Bellarbarba et al., 2008; Tang et al., 2012; Loizzo et al., 2013); however, the isolation scanner with mechanical rotation and the subsequent data interpretation are complex to use and perform. The acoustic wavefield and detection methods are being studied theoretically to better evaluate the cement bond quality (Tubman et al., 1984, 1986; Song et al., 2012; Duan et al., 2014; He et al., 2014).

Qiao et al. (2006) presented a new type of downhole transmitter and Qiao et al. (2008) investigated the radiation directivity of an acoustic phased-arc array. Subsequently, the acoustic field generated by phased-arc arrays in open and cased boreholes was simulated (Che and Qiao, 2009; Che et al., 2014). These authors showed that the acoustic phased-arc array transmitter offers several advantages over conventional monopole sources. A source with directional radiation properties in a cased hole is a new well logging tool with azimuthal resolution suitable for cased holes. Based on field applications and requirements, we used the phased-arc array transmitter in the azimuthally acoustic bond tool (AABT). Lu et al. (2014) presented detailed electronic systems and laboratory measurements of the AABT. To assess the performance of the AABT, we simulated the acoustic field of the AABT in cased holes. We investigated the response characteristics of channeling and the radiation azimuth using a parallel 3D finite-difference algorithm. We tested the AABT in several wells to verify its performance and to obtain the azimuthal sensitivity.

Acoustic sonde of the AABT

The acoustic sonde of the AABT is shown schematically in Figure 1a. The acoustic sonde typically has one acoustic phased-arc array transmitter (T) and two monopole receivers (R_1 and R_2), which are placed 3 ft (0.91 m) and 5 ft (1.52 m) away from the transmitter, respectively. Figure 1b shows the AABT, which mainly consists of a transmitter, two receivers, an isolator, and an electronic section. The acoustic phased-arc array transmitter consists of eight piezoelectric ceramic vibrators evenly distributed on a circle and operating at center frequency of 15 kHz. The operating principle of the transmitter is similar to that of Che and Qiao (2009). Each vibrator can function as an element of the acoustic phased-arc array. The main advantage of the acoustic phased-arc array is its capability to radiate energy into different azimuths at different times. When all eight vibrators are excited simultaneously, the acoustic phased-arc array transmitter works similarly to a conventional monopole transmitter. In this work, we choose three neighboring vibrators to work as a phased-arc subarray. Different vibrators are operated in sequence to radiate acoustic energy into the borehole wall at different azimuths by excitation circuits. At each measurement depth, two receivers at 3 ft and 5 ft intervals acquire sixteen tracks of waveforms.

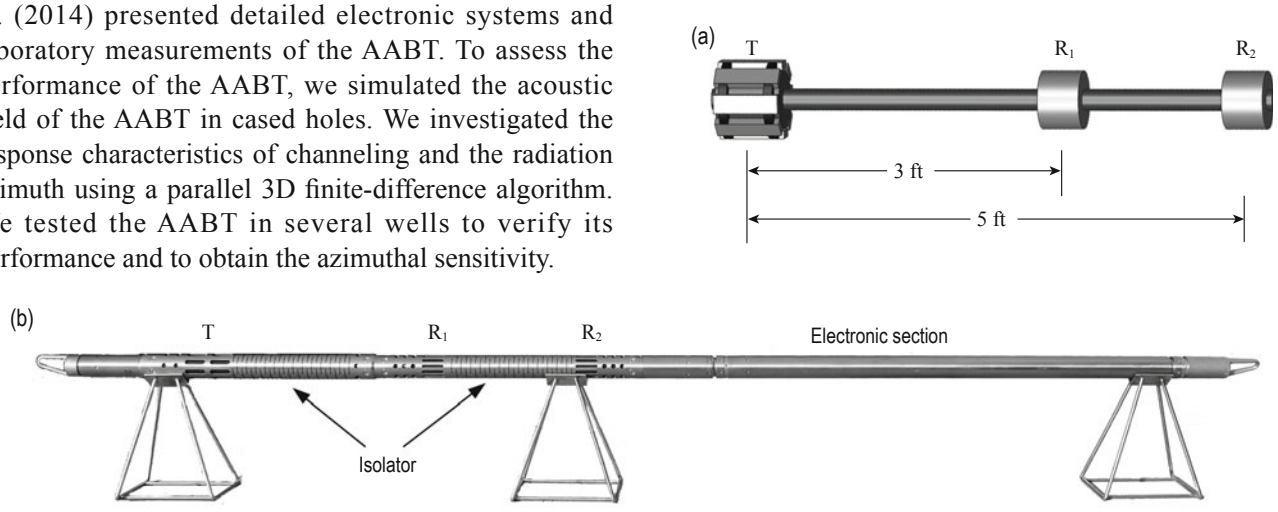

Fig.1 (a) Schematic of the acoustic sonde and (b) photo of the AABT. The AABT consists of a transmitter (T), two receivers (R_1 and R_2), an isolator, and an electronic section.

Numerical simulation

The finite-difference method is widely used in numerical simulations of borehole acoustic fields. We use a 3D finite-difference scheme (Cheng et al., 1995; Liu et al., 1996) in Cartesian coordinates to simulate the acoustic field for a variety of AABT models on a cluster.

We study the effect of the channeling circumference size and the radiation azimuth on the casing waves.

We first define the densities, Lamé constants, particle velocities, and stress for homogeneous media. The elastic equations are then decomposed into first-order partial differential equations of velocity and stress (Che and Qiao, 2009). The partial differential equations are substituted by differential schemes after discretization. The elastic equations, stiffness coefficients, densities and the splitting perfectly matched layer (PML) are referred to former studies (Che and Qiao, 2009; He and Hu, 2009; He et al., 2010).

The AABT models

We simulated the acoustic characteristics of the casing waves with the AABT for different cement bonding conditions. We call the numerical calculation models "the AABT models". As shown in Figure 2a, the AABT numerical simulation model consists of an innermost fluid cylinder surrounded by the casing pipe, cement annulus, and formation. T represents the acoustic phased-arc array transmitter with eight elements, and R_1 and R_2 are the monopole receivers. The distance from T to R_1 and R_2 is 3 ft and 5 ft, respectively. We assume a 0.5 m high channeling with sector β in the cement between T and R_1 (Figure 2b). The height and outer diameter of the model well are 3.8 m and 1.0 m, respectively. The radius of the borehole is 0.1 m. The casing pipe thickness is 0.01 m and the cement annulus thickness is 0.02 m. The P-wave and S-wave velocities and densities for each material are listed in Table 1. The radiation azimuth of the phased-arc array transmitter is α. We simulated many models, where we varied the circumferential channeling size β while keeping the other parameters constant. For each model with a given channeling size, we change the radiation azimuth of the transmitter at α of 0°, 45°, 90°, 135°, 180°, 225°, 270°, and 315°.

Table 1 Parameters of the materials used in the simulations

	Casing pipe	Cement annulus	Formation	Borehole fluid
VP (m/s)	5900	3500	4000	1500
VS (m/s)	3230	2000	2500	–
ρ (kg/m^3)	7800	1900	2200	1000

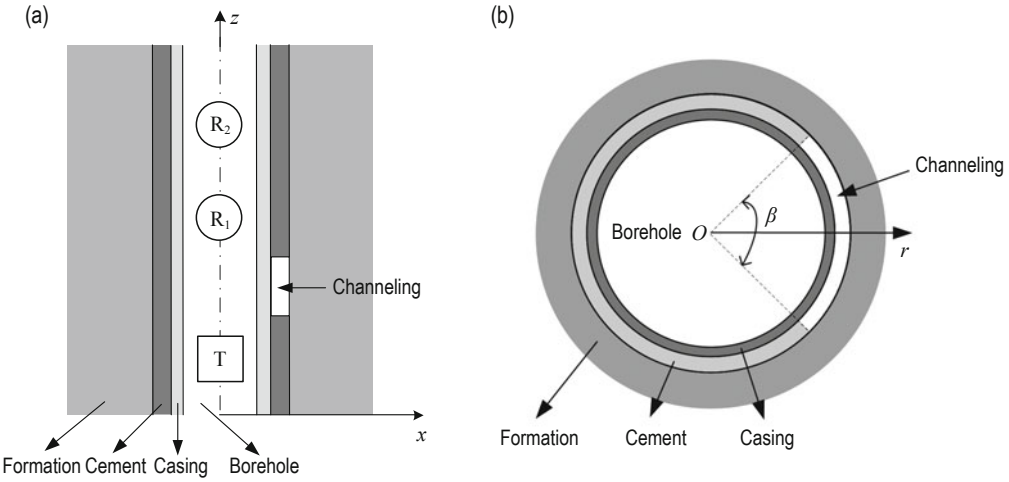

Fig.2 Schematic of the AABT model: (a) vertical section and (b) horizontal section at the channeling position.

Simulation results

The acoustic waveforms received by R_1 and R_2 are shown in Figure 3 for $\beta = 90°$ and, with the eight three-element arc subarrays scanning the radiation acoustic energy in the cased hole every 45°, these eight acoustic waveforms correspond to α of 0°, 45°, 90°, 135°, 180°, 225°, 270°, and 315°. Figure 4 shows the relation between the amplitude of the first arrival and the radiation azimuths for $\beta = 90°$. The amplitudes of the first arrivals from R_1 and R_2 have differences owing to channeling. The radiation azimuth of the transmitter corresponding to the maximum amplitude of the first arrival faces the azimuth of the channeling exactly. The amplitude differences of the first arrivals among the different radiation azimuths from R_1 are relatively greater than from R_2.

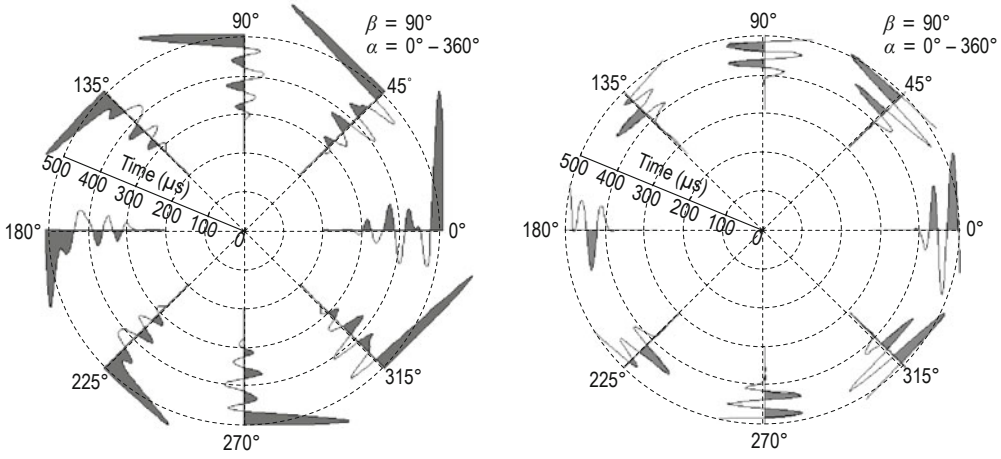

(a) R_1 (b) R_2

Fig.3 Eight acoustic waveforms generated by the eight three-element arc subarrays scanning the radiation acoustic energy in the borehole every 45° for β = 90°.

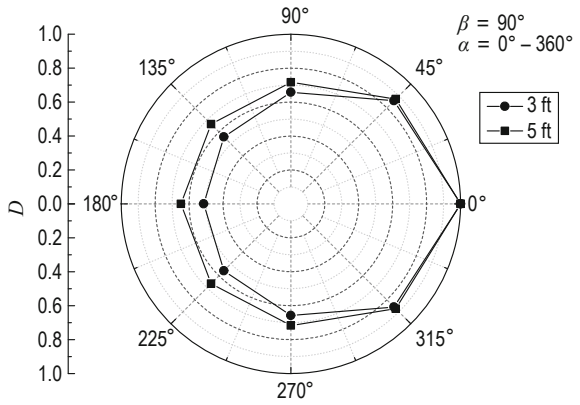

Fig.4 Relation between the amplitude of the first arrival and the radiation azimuths for β = 90°. D is a dimensionless variable.

We also simulated the acoustic waveforms for different channeling circumferences. Figure 5 shows the relation between the amplitude of the first arrival from R_1 and R_2 and the radiation azimuths for β of 90°, 45°, 27°, and 0°. The figure shows that the amplitude difference of the casing wave is more apparent in Figure 5a than in 5b, and that the larger circumference of the channeling produces greater amplitude differences of the casing wave. For the cases of free casing and good cementing, the amplitude of the casing wave does not change with the radiation azimuth of the three-element subarrays. The calibrated relative amplitude normalized by the amplitude of free casing wave can distinguish the two special conditions.

The numerical results show that the eight waveforms and the amplitude of the first arrival are different when there is a channeling behind the casing at specific azimuth. This is the basis for the azimuthal evaluation of cement bonding at the casing–cement interface. Similarly, the formation wave generated by the phased-arc array also shows azimuthal variation if there is a

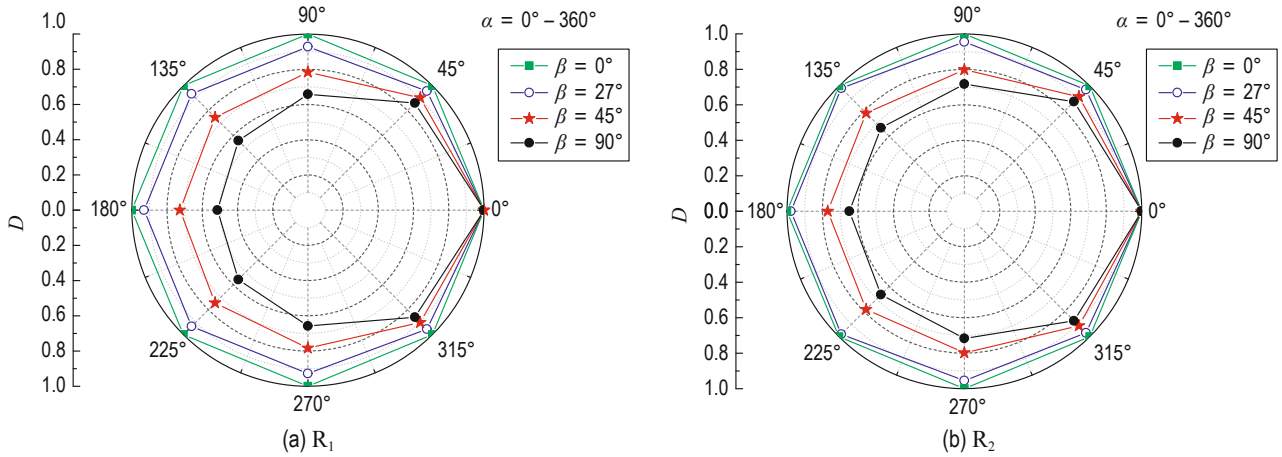

(a) R_1 (b) R_2

Fig.5 Relation between the amplitude of the first arrival and azimuth for β of 0°, 27°, 45°, and 90°. D is a dimensionless variable.

channeling. As a result, the cement bond quality at the cement–formation interface can be azimuthally evaluated according to the azimuthal difference in amplitude and arrival time. The AABT was extensively tested in test and commercial wells in China.

Data processing of the phased-arc array logging

The amplitude of the first arrival, the attenuation of the first arrival, and the amplitude of the formation wave can be extracted and imaged using the eight waveforms acquired by each receiver from the different radiation azimuths. Furthermore, the cement bond quality at the casing–cement interface and the cement–formation interface can be evaluated using the amplitude and attenuation of the first arrival and the formation wave. If there are inconsistencies among the eight vibrators of the transmitter, it is necessary to correct it before extracting the amplitude of the first arrival and the formation wave. We assume the correction coefficient for the transmitter is C_i and the amplitude before correction is B_i ($i = 1 - 8$), where i is the phase-arc array element number, and the amplitude after correction is A_i ($i = 1 - 8$)

$$A_i = B_i \times C_i, \ (i = 1 - 8), \tag{1}$$

where C_i can be determined by experimental measurements or data from calibration wells. We obtain the amplitude curves for the eight radiation azimuths using the waveforms received by the receivers spaced at 3 ft and 5 ft, respectively. The amplitude map of the first arrival with azimuthal resolution is achieved using 360° interpolation. We calculate the attenuation coefficients from the amplitudes of the first arrival from the receivers at 3 ft and 5 ft using the following equation

$$\alpha = 20\log_{10}\left(\frac{A_{3\text{ft}}}{A_{5\text{ft}}}\right) / 0.6096, \tag{2}$$

where α is the attenuation coefficient of the casing wave, $A_{3\text{ft}}$ and $A_{5\text{ft}}$ are the amplitudes of the first arrivals from the receivers at 3 ft and 5 ft, respectively. The attenuation map of the first arrival with azimuthal resolution is imaged using the eight coefficients interpolated in 360°. The amplitude map and the attenuation map are highly correlated; the larger amplitude of the first arrival corresponds to the lower attenuation coefficient and vice versa. Both the attenuation and amplitude maps can be used in evaluating the cement bonding. However, in the good cement bond condition at the casing–cement interface, the amplitude of the casing wave is too weak to be accurately identified, which results in unreliable attenuation coefficients. Therefore, the additional arrival time of the first arrivals can be used to indicate the cement bonding conditions at the casing–cement interface.

In the good casing–cement bond condition, we can evaluate the cement bonding at the cement–formation interface by using the amplitude of the formation wave from the receiver of the AABT at 5 ft spacing. To improve the accuracy of the amplitude extraction, we preprocess the raw data. We use phase tracking to demarcate the travel time of the formation wave from different radiation azimuths at different depths and we then determine the start position of the window on the waveforms. The F–K transformation (Mou, 1993) or the medium-filtering method (Zhu, 1992) can be used to suppress the casing waves, which increase the S/N of the formation waves. The Hilbert transform (Hu, 2003) of the preprocessed waveforms yields the transient amplitude spectrum. We open a window on the transient amplitude spectrum and extract the amplitude of the formation wave. Then, we image the amplitude of the formation wave with azimuthal resolution using the eight amplitude curves.

In addition to showing the AABT measurements, we also show the amplitude curve and the variable density log, as in conventional CBL and VDL. According to the superposition theory of acoustic wave fields, the waveforms with spacings of 3 ft and 5 ft can be obtained by the weighted average of the eight waveforms from different radiation azimuths. Furthermore, we calculate the amplitude of the first arrival to determine the amplitude curve as in conventional CBL after the normalization by the amplitude of the free casing. Similarly, we show the variable density as in conventional VDL, after processing the waveforms acquired by the receivers at 5 ft spacing.

Field tests and case study

We study and analyze the data for free casing, casing –cement interface, and cement–formation interface to obtain the acoustic characteristics and interpretation methods for different cement bonding conditions with phased-arc array logging.

Free casing

The AABT was tested in a well in northern China and the data are shown in Figure 6. The left two tracks show the GR and the depth. The third track shows the

amplitudes of the first casing arrivals; AMP1 to AMP8 are the amplitudes from eight different radiation azimuths recorded by the receivers spaced at 3 ft. The fourth track, labeled as AMPMAPI, is the amplitude map of the first arrival from AMP1 to AMP8 with 360° interpolation. The fifth track shows the maximum, the average, and the minimum amplitude of the casing arrival as well as the CBL amplitude curve. The CBL amplitude curve in track 5 is similar to the conventional CBL. The two tracks on the right are the waveforms and the variable density recorded by the receivers at 3 ft spacing.

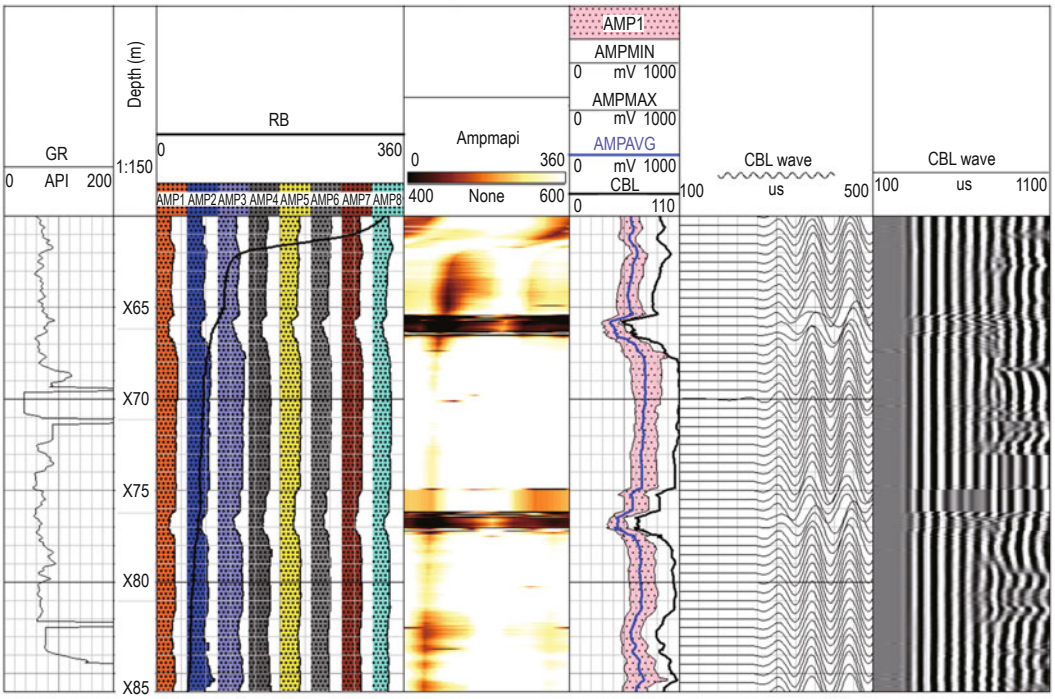

Fig.6 Measurements of the AABT logged in the case of free casing in northern China.

As shown in Figure 6, the baselines of the waveforms are stable with high S/N. The first arrivals are casing waves with constant arrival time and high amplitudes, which produce the black and white stripes in the variable density. The black and white stripes do not change with depth except at the collars. We can easily locate the casing collars in track 4. The imaged casing collars are characterized as dark stripes with deep and even color in the circumferential direction. The variable density display also shows the amplitude attenuation as well as the arrival time delays.

Evaluation at the casing-cement interface

The azimuthal characteristics of the first arrival enable us to evaluate the cement bond quality at the casing–cement interface with azimuthal resolution. Figure 7 shows the measurements logged by the AABT in one well in western China. The left five tracks correspond to the GR, the depth, the map of the arrival time for the first arrival, the amplitude map of the first arrival, and the attenuation map of the first arrival. The sixth track shows the maximum, the minimum, and the average arrival time for the first arrival. The seventh track shows the maximum, the minimum, and the average amplitude of the casing arrival combined with the CBL amplitude curve. The eighth track shows the maximum, the minimum, and the average attenuation of the first arrival. The three tracks on the right are the waveforms, the variable density recorded by the receivers at 3 ft spacings, and the variable density recorded by the receivers at 5 ft spacings.

As shown in Figure 7, the high amplitude values of the first arrival correspond to low values on the arrival time and attenuation curves, which suggest bad cement bonding at the casing–cement interface. In contrast, the low amplitude values of the first arrival correspond to high values on the arrival time and the attenuation curves, which suggest good cement bonding at the casing –cement interface. At the depths where the bonding between the casing and cement is good, the extracted arrival time curve and the attenuation curve of the first arrival are from the formation wave. This is because

the casing waves have very low amplitudes, which are difficult to detect accurately. In these cases, the arrival time curve and the attenuation curve are not suitable for evaluating the cement bonding at the casing–cement interface. Between X05 m and X12 m, the measurements show that the amplitude of the first arrival is very low and the arrival time is relatively late, which points to good cement bonding at the casing–cement interface.

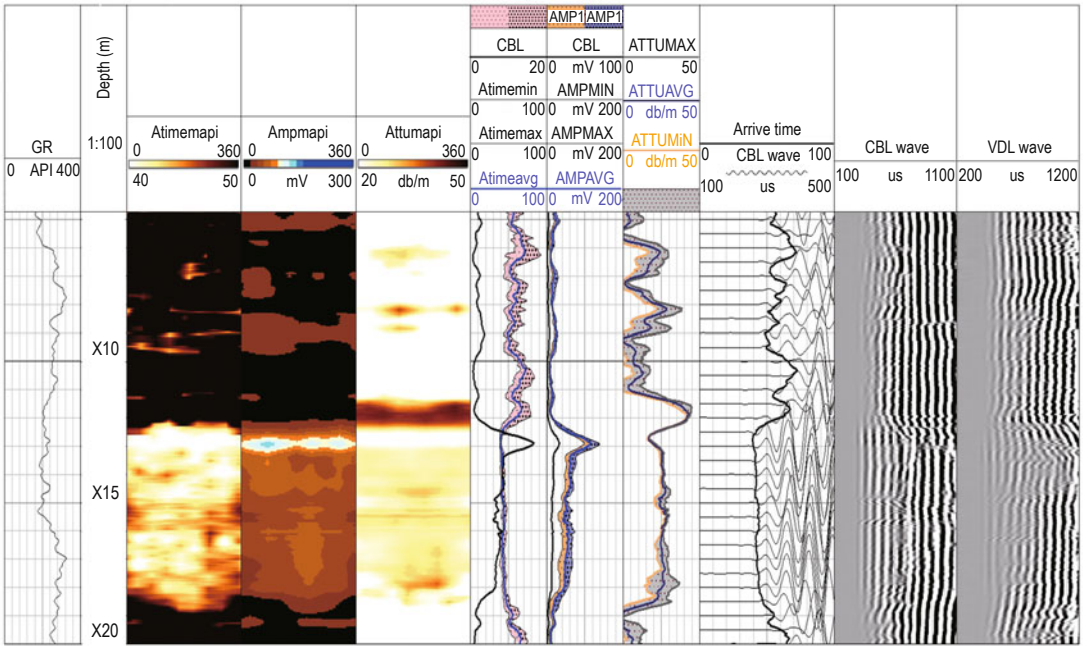

Fig.7 Evaluation at the casing-cement interface by the AABT in western China.

Evaluation at the cement-formation interface

The azimuthal characteristics of the formation wave allow the azimuthal evaluation of cement bonding at the cement–formation interface. Figure 8 shows the AABT measurements from a well in northern China. The left two tracks show the GR and the depth. The third track shows the amplitudes of the formation wave; AMP1 to AMP8 are the amplitudes from eight different radiation azimuths recorded by the 5-ft-spacing receiver. The fourth and fifth tracks show the amplitude map of the formation wave and the amplitude map of the first arrival. The sixth track shows the maximum, the minimum, and the average amplitude of the casing arrival as well as the CBL amplitude curve. The two tracks on the right are the waveforms and the variable density display recorded by the receiver at 5 ft spacing.

When the cement bonding at the casing–cement interface is poor, the amplitude of the formation wave is lower than that of the casing wave. In this case, the formation wave cannot be extracted accurately, as shown in the interval X912 m to X913 m. The amplitude variations shown in the amplitude map of the formation wave are consistent with those in the amplitude map of the first arrival; this correlation is explained by the amplitude map of the formation wave that reflects the contribution of the significantly large amplitude of the casing wave. In this case, the map of the formation wave cannot be used to interpret the cement bonding conditions at the cement–formation interface.

When the cementing at the casing–cement interface is fair and the casing waves have almost no effect on the extraction of the amplitude of the formation wave, the pattern in the amplitude map of the formation wave and that in the amplitude map of the first arrival from X915 m to X918 m are almost opposite to each other. For excellent cement bonding at the casing–cement interface, the casing waves are hardly observable in the waveforms. The azimuthal characteristics of the amplitude of the formation wave significantly contribute to the evaluation of the cementing at the cement–formation interface. From X910 m to X912 m, the amplitude of the casing wave is small, even in the circumferential direction, whereas the amplitude of the formation wave is small, uneven in the circumferential direction; thus, indicating that the casing–cement bonding is good but a channeling or an aperture exists between the cement and the formation.

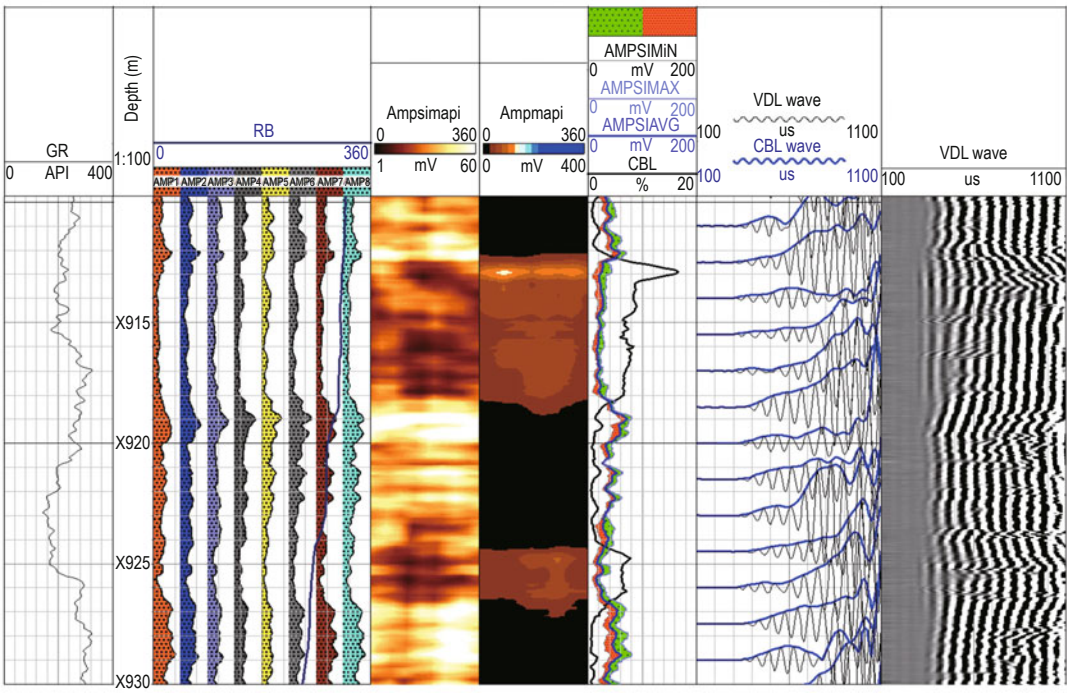

Fig.8 A case for evaluation at the cement-formation interface by the AABT in northern China.

Conclusions

The phased-arc array transmitter is an innovative downhole source that can radiate acoustic energy around the circumference of the borehole wall in a narrow angle range. We use these attributes to design and develop a new cementing logging tool named AABT with a phased-arc array transmitter and build a cement evaluation system with azimuthal resolution. The AABT operates at 15 kHz and contains source–receiver systems at 3 ft and 5 ft spacings, which are designed to improve the conventional CBL and VDL. The combination of numerical simulation and field tests enable us to verify the characteristics and functions of the AABT.

We modeled the source–receiver system of the AABT in a cased borehole surrounded by layered materials with a channeling inside the cement annulus at specific azimuth. Each receiver records eight waveforms corresponding to eight different radiation azimuths of the phase-arc array transmitter. The waveforms and amplitudes of the first arrival from different radiation azimuths are different when the channeling is behind the casing, which can be used to evaluate the cement bonding with azimuthal resolution. We also find that when the main acoustic radiation beam is close to the channeling, the amplitude of the casing wave increases significantly, and the radiation azimuth that corresponds to the maximum amplitude of the casing wave faces the channeling azimuth.

The AABT was tested in several wells in western and northern China. We processed the measured data and found that the AABT can accurately locate collars. The AABT can use the amplitude map and the arrival time of the first arrival to azimuthally evaluate the bonding at the casing–cement interface. When the casing–cement bonding is good, the AABT can also azimuthally visualize the cement bonding at the cement–formation interface by using the amplitude map of the formation wave. The two tool spacings are as in the CBL or VDL; therefore, the 3 ft spacing of the tool is equivalent to the azimuthal CBL and the 5 ft spacing is equivalent to the azimuthal VDL. The azimuthal resolution of the AABT depends on the bandwidth of the acoustic radiation beam.

Acknowledgements

The authors would like to thank the editors and reviewers for their valuable comments. The authors are also grateful to Wenxing Duan at China University of Petroleum, Beijing and Yunyue Li at Massachusetts Institute of Technology for their help in drawing the figures and English. Che X. H. was supported from the China Scholarship Council (No. 201306445018) and the

Earth Resources Laboratory at Massachusetts Institute of Technology (MIT) through a visiting scientist opportunity in 2014–2015, and wishes to thank Prof. M. N. Toksöz for his support and help during the visit at MIT.

References

Bellabarba, M., Bulte-Loyer, H., and Froelich, B., et al., 2008, Ensuring zonal isolation beyond the life of the well: Oilfield Review, **20**, 18–31.

Bigelow, E. L., Domangue, E. J., and Lester R. A., 1990, A new and innovative technology for cement evaluation: 65th Annual Technical Conference and Exhibition of the SPE 20585.

Bolshakov, A., Dubinsky, V., Tang X. M., et al., 2010, Casing resonant radial flexural modes in cement bond evaluation: U. S. Patent **7**, 681, 450.

Che, X. H., and Qiao, W. X., 2009, Numerical simulation of an acoustic field generated by a phased arc array in a fluid-filled borehole: Petroleum Science, **6**(3), 225–229.

Che, X. H., Qiao, W. X., Wang, R. J., et al., 2014, Numerical simulation of an acoustic field generated by a phased arc array in a fluid-filled cased borehole: Petroleum Science, **11**(3), 385–390.

Cheng, N. Y., Cheng, C. H., and Toksöz, M. N., 1995, Borehole wave propagation in three dimensions: Journal of the Acoustical Society of America, **97**, 3483–3493.

Duan, W. X., Qiao, W. X., Che, X. H., et al., 2014, Acoustic evaluation of cementing quality using obliquely incident ultrasonic signals: Applied Geophysics, **11**(3), 269–276.

He, X. and Hu, H. S., 2009, Borehole flexural modes in transversely isotropic formations: the low-frequency asymptotic velocity: Geophysics, **74**(4), E149–E158.

He, X., Hu H. S., and Guan, W., 2010, Fast and slow flexural waves in a deviated borehole in homogeneous and layered anisotropic formations: Geophysical Journal International, **181**(1), 417–426.

He, X., Chen, H., and Wang, X. M., 2014, Ultrasonic leaky flexural waves in multilayered media: cement bond detection for cased wellbores: Geophysics, **79**(2), A7–A11.

Hu, G. S., 2003, Digital signal processing: Tsinghua University press, second edition.

Liu, Q. H., Schoen, E., Daube, F. et al., 1996, A three-dimensional finite difference simulation of sonic logging: Journal of the Acoustical Society of America, **100**, 72–79.

Loizzo, M., Miersemann, U., Lamy, P., et al., 2013, Advanced cement integrity evaluation of an old well in the Rousse field: Energy Procedia, **37**, 5710–5721.

Lu, J. Q., Ju, X. D., Qiao, W. X., et al., 2014, Azimuthally acoustic logging tool to evaluate cementing quality: Journal of Geophysics and Engineering, **11**(4), 1–12.

Mou, Y. G., 1993, Digital processing method of the seismic data: Petroleum Industry press.

Pardue, G. H., Morris, R. L., Gollwitzer, L. H., et al., 1963, Cement bond log-a study of cement and casing variables: Journal of Petroleum Technology, **15**(5), 545–555.

Qiao, W. X., Ju, X. D., Chen, X. L., et al., 2006, Downhole acoustic arc array transmitter with controlled azimuthal directivity: China Patent 03137596. 0.

Qiao, W. X., Che, X. H., Ju, X. D., et al., 2008, Acoustic logging phased arc array and its radiation directivity: Chinese Journal of Geophysics, **51**(3), 939–946.

Qiao, W. X., Ju, X. D., Che, X. H., et al., 2011, Progress in acoustic well logging technology: Well Logging Technology, **35**(1), 14–19.

Schlumberger, http://www.slb.com/~/media/Files/cementing/product_sheets/isolation_scanner.pdf.

Song, R. L., Liu, J. X., Hou, C. H., et al., 2012, Numerical simulation of Sector Bond log and improved cement bond image: Geophysics, **77**(4), no. 4, D95–D104.

Tubman, K. M., Cheng, C. H., Cole, S. P., et al., 1986, Synthetic full-waveform acoustic logs in cased boreholes, II — poorly bonded casing: Geophysics, **51**(4), 902–913.

Tubman, K. M., Cheng, C. H., and Toksoz, M. N.. 1984, Synthetic full waveform acoustic logs in cased boreholes: Geophysics, **49**(7), 1051–1059.

Tang, H. P., Zhang, H. T., and Li, G. R., 2012, Applications of isolation scanner (IBC) imaging logging in horizontal well: Journal of Oil and Gas Technology, **34**(8), 88–93.

van Kuijk, R., Zeroug, S., Froelich, B., et al., 2005, A novel ultrasonic cased-hole imager for enhanced cement evaluation: International Petroleum Technology Conference.

Zhu, G. M., 1992, Vertical seismic profile method, Petroleum Industry Press.

Che Xiao-Hua is an associate professor at China University of Petroleum, Beijing. She received her Ph.D. (2003) in Geological Resources and Geological Engineering from China University of Petroleum. Her research interests are acoustic well logging and laboratory experiments.